OPEN ACCESS

Original research

Microstructural plasticity in nociceptive pathways after spinal cord injury

Sreenath P Kyathanahally,[1] Michela Azzarito,[1] Jan Rosner ,[1,2] Vince D Calhoun,[3] Claudia Blaiotta,[4] John Ashburner,[4] Nikolaus Weiskopf,[5] Katja Wiech,[6] Karl Friston,[4] Gabriel Ziegler,[7] Patrick Freund [1,4,5]

► Additional supplemental material is published online only. To view, please visit the journal online (http://dx.doi.org/10.1136/jnnp-2020-325580).

For numbered affiliations see end of article.

Correspondence to
Professor Patrick Freund, Wellcome Centre for Human Neuroimaging, UCL Institute of Neurology, London WC1N 3BG, UK; patrick.freund@balgrist.ch

SPK, MA and JR contributed equally.

Received 5 November 2020
Revised 12 March 2021
Accepted 21 April 2021
Published Online First 26 May 2021

ABSTRACT

Objective To track the interplay between (micro-) structural changes along the trajectories of nociceptive pathways and its relation to the presence and intensity of neuropathic pain (NP) after spinal cord injury (SCI).

Methods A quantitative neuroimaging approach employing a multiparametric mapping protocol was used, providing indirect measures of myelination (via contrasts such as magnetisation transfer (MT) saturation, longitudinal relaxation (R1)) and iron content (via effective transverse relaxation rate (R2*)) was used to track microstructural changes within nociceptive pathways. In order to characterise concurrent changes along the entire neuroaxis, a combined brain and spinal cord template embedded in the statistical parametric mapping framework was used. Multivariate source-based morphometry was performed to identify naturally grouped patterns of structural variation between individuals with and without NP after SCI.

Results In individuals with NP, lower R1 and MT values are evident in the primary motor cortex and dorsolateral prefrontal cortex, while increases in R2* are evident in the cervical cord, periaqueductal grey (PAG), thalamus and anterior cingulate cortex when compared with pain-free individuals. Lower R1 values in the PAG and greater R2* values in the cervical cord are associated with NP intensity.

Conclusions The degree of microstructural changes across ascending and descending nociceptive pathways is critically implicated in the maintenance of NP. Tracking maladaptive plasticity unravels the intimate relationships between neurodegenerative and compensatory processes in NP states and may facilitate patient monitoring during therapeutic trials related to pain and neuroregeneration.

INTRODUCTION

The underlying pathophysiology of neuropathic pain (NP) after spinal cord injury (1) is complex and involves alterations within 'bottom-up' nociceptive processing (ie, afferent integrity) and 'top-down' endogenous pain modulation.[1] Functional changes within descending modulatory pathways have been related to the presence of NP after spinal cord injury (SCI).[2] The descending pain modulatory network encompasses a cortical–subcortical–brainstem network involved in the modulation of afferent nociceptive information.[3] Key constituents involved in nociceptive information processing are the posterior insula, thalamus, periaqueductal grey (PAG), the anterior cingulate cortex (ACC) and dorsolateral prefrontal cortex (DLPFC) (for review, see Wiech[4]). Within ascending nociceptive pathways, inhibition and facilitation of afferent input already occurs at the level of the dorsal horn where primary afferent fibres synapse onto projection neurons.[5] Modulatory changes within these regions can precipitate a pro-nociceptive state and potentially contribute to the emergence and chronification of NP.[6] Traumatic SCI triggers a cascade of trauma-induced secondary neurodegenerative processes, involving demyelination and iron accumulation in the spinal cord and brain,[7] which can be tracked using quantitative MRI (qMRI).[8] To date, increases and decreases in brain and cord macrostructural (ie, volumetric) changes have been associated with the occurrence of NP.[9] Moreover, macrostructural tissue sparing (ie, ventral tissue bridges) could be related to the emergence and maintenance of NP after SCI.[10] However, microstructural correlates of these NP associated processes within areas undergoing atrophy and beyond are understudied. Based on recent studies illustrating that activity-dependent plasticity can translate into changes in myelin architecture, we hypothesised that such pathophysiological processes will be reflected in microstructural changes to myelin and iron content along nociceptive pathways.

We used a multi-parametric mapping (MPM) protocol[8] that provides contrasts that are sensitive to myelination (via magnetisation transfer (MT) saturation, longitudinal relaxation (R1)[11 12]), and sensitive to iron content in tissue as well as in blood (using the effective transverse relaxation rate (R2*)[13]) to track the complex relationship between structural and metabolic changes along the trajectories of nociceptive pathways and its relation to the presence and intensity of NP. To characterise simultaneously NP related changes across the neuraxis, we used a combined brain and spinal cord template[14] embedded in the statistical parametric mapping (SPM) framework. Finally, we applied multivariate source-based morphometry (SBM), which estimates interrelationships among voxels across the neuraxis to identify naturally grouped patterns of structural variation between groups.[15] The multivariate (SBM) tests for group effects are, in principle, much more sensitive than the equivalent mass univariate (voxel-based morphometry (VBM)) tests one would obtain from analysing the volumetric and microstructural images directly.

Check for updates

© Author(s) (or their employer(s)) 2021. Re-use permitted under CC BY-NC. No commercial re-use. See rights and permissions. Published by BMJ.

To cite: Kyathanahally SP, Azzarito M, Rosner J, *et al*. *J Neurol Neurosurg Psychiatry* 2021;**92**:863–871.

J Neurol Neurosurg Psychiatry: first published as 10.1136/jnnp-2020-325580 on 26 May 2021. Downloaded from http://jnnp.bmj.com/ on July 20, 2021 at E-Library Insel. Protected by copyright.

Table 1 Participant characteristics

	SCI-NP (n=13)	SCI-nNP (n=17)
Age (years)	42.9±18.2	46.1±14.8
Sex (%)		
Male	85	94
Female	15	6
Level of injury (%)		
Tetraplegia	62	35
Paraplegia	38	65
AIS grade (%)		
A	23	59
B	31	18
C	8	0
D	38	23
Neuropathic pain		
At level (%)	55	–
Below level (%)	55	–
NRS* (0–10)	6.1±1.9	–
ISNCSCI scores		
Pinprick (0–122)	60.2±30.2	56.3±25.4
Light touch (0–122)	70.9±24.4	66.4±26.2
Motor (0–100)	59.2±26.3	56.2±25.1

Data are shown as mean±SD or percentage (as indicated).
*Average pain intensity during the last week.
AIS, American Spinal Cord Injury Association (ASIA) Injury Severity at baseline; ISNCSCI, International Standards for Neurological Classification of Spinal Cord Injury; NRS, Numerical Rating Scale; SCI-nNP, individuals with spinal cord injury without neuropathic pain; SCI-NP, individuals with spinal cord injury and neuropathic pain.

This is because multivariate analyses do not try to assign a significance to each voxel or region—they test for distributed effects that covary among individuals.[16] Due to SBMs sensitivity to minute changes, this approach was chosen to detect microstructural changes. To dissociate NP-associated changes from trauma-induced changes we first compared MRI indices between SCI patients with and without NP and then between SCI patients and healthy controls.

MATERIALS AND METHODS

Participants

Thirty chronic traumatic SCI patients (13 with and 17 without NP (table 1)) and 23 healthy controls participated in the study (online supplemental S1). These participants were also enrolled in a longitudinal study.[17–19] Eligible individuals with a traumatic SCI and healthy controls were older than 18 years, and had no history of head and brain lesions, no pre-existing neurological, mental or medical disorders affecting outcome, and no contra-indications to MRI.

CLINICAL ASSESSMENT

The neurological examination was performed according to the International Standards for Neurological Classification of Spinal Cord Injury.[20] The pain intensity was quantified using an 11-point numeric rating scale with '0' indicating no pain and '10' indicating the worst imaginable pain. NP was defined according to the standard taxonomy related to SCI,[21] which required its presence in an area of sensory deficit (at or below the lesion level) and other causes like musculoskeletal pain had to be ruled out during the clinical assessment. We used ANOVA tests to assess group differences for the demographics (ie, lesion level, American Spinal Cord Injury Association (ASIA) Injury Severity at baseline (AIS) grade).

DATA ACQUISITION

Structural whole-brain data, including the cervical cord down to vertebra C5, were acquired on a 3T Magnetom-Verio MRI scanner (Siemens Healthcare, Erlangen, Germany) equipped with a 16-channel radiofrequency (RF) receive head and neck coil and RF body transmit coil. The scanner was upgraded during the study period (from Verio to Skyra^{fit}) which resulted in 15 controls and 20 patients being scanned on the Verio and 8 controls and 10 patients being scanned on the Skyra system.

A T1-weighted (T1w) structural scan was acquired using a 3D MPRAGE (magnetisation-prepared rapid acquisition gradient echo) sequence with the following: field of view (FoV) of 224×256×176 mm^3, matrix size 224×256×176, isotropic resolution of 1 mm^3, repetition time (TR)=2420 ms, echo times (TE)=4.18 ms, flip angle (α)=9°, inversion time=960 ms, and readout bandwith of 150 Hz per pixel.

A whole-brain multi-parameter mapping (MPM) qMRI protocol,[22] using a multi-echo 3D FLASH (fast low-angle shot) sequence, was performed. The following parameters were used: FoV of 240×256×176 mm^3, matrix size=240×256×176, isotropic resolution of 1 mm^3, GRAPPA parallel imaging in phase-encoding direction (anterior–posterior) with speed-up factor of 2, partial Fourier acquisition with 6/8 sampling factor in the partition direction (left–right) and a readout bandwidth of 480 Hz per pixel. Differently weighted MRI images were achieved by choices of TR and flip angle (α): (1) T1 weighted (T1w): 25 ms/23°, (2) PD weighted (PDw): 25 ms/4° and (3) MT weighted (MTw): 37 ms/9° with off-resonance MT saturation RF pulse prior to excitation. This MT pulse consists of a Gaussian shaped off resonance pulse at 1.2 kHz with length 10 ms, pulse angle 500° and MT pulse bandwidth of 192 Hz. Echoes were acquired at seven equidistant TE, from 2.46 ms to 17.22 ms for all volumes and an additional echo at 19.68 ms for PDw and T1w.

DATA ANALYSIS

We used SPM12 spatial routines on the T1w images and MPM maps. As a novelty, we used a brain plus spinal cord (BSC) template[23] covering the brain and the upper cervical spinal cord in the unified segmentation approach,[24] which allowed us to assess brain and cervical cord changes within the same statistical framework. This BSC template was specified as a *tissue probability map* (ie, spatial prior) in the unified segmentation step. This procedure assumes every voxel to be drawn from an unknown mixture of 12 Gaussians, which were grouped into seven distinct tissue classes: grey matter (GM, using one Gaussian), white matter (WM, using one Gaussian) and cerebrospinal fluid (using one Gaussian), bone and air (using three Gaussians), soft tissue (using three Gaussians), non-neural tissues (using three Gaussians) and air/background (using three Gaussians).[24] For volumetric analysis, we applied SPM12's unified segmentation, including the BSC template, to each subject's MPRAGE image (ie, T1w). T1w images were non-linearly transformed into standard MNI (Montreal Neurological Institute) space using diffeomorphic group-wise registration (Dartel) implemented in SPM12.[25] This defined the space for subsequent modelling steps. Finally, GM and WM probability maps were smoothed with an isotropic Gaussian kernel of 5 mm full width at half maximum.

For microstructural analysis, the acquired T1w, PDw and MTw FLASH echoes from the MPM protocol, were first

J Neurol Neurosurg Psychiatry: first published as 10.1136/jnnp-2020-325580 on 26 May 2021. Downloaded from http://jnnp.bmj.com/ on July 20, 2021 at E-Library Insel. Protected by copyright.

averaged to increase signal to noise ratio. Unified segmentation based correction of R1 brain maps for RF transmit field inhomogeneities (UNICORT) was then used for correcting RF transmit field inhomogeneity and to calculate quantitative maps of MT saturation, R1 and R2*.[8] MT maps were segmented using the unified segmentation approach that included the BSC template.[14] Segmented MT maps were then transformed non-linearly to standard MNI space using Dartel, but without scaling by the Jacobian determinants (ie, no 'modulation' of parameter values). Additionally, all MPM maps (MT, R1 and R2*) were warped to the MNI space by using the participant specific flow fields from the MT maps and finally smoothed using a previously established tissue-weighted-smoothing procedure with a kernel of 5 mm, in order to preserve quantitative values within the GM and WM tissue classes of each MPM map.

Subsequent modelling and analysis were performed for smoothed, normalised morphometric and microstructural parameter images (for WM and GM) across the brain and cervical cord, simultaneously. Each of the morphometric and microstructural parameter images were then individually analysed using SBM.[16] SBM[16] is a multivariate analysis approach, implemented in the SBM toolbox within Group ICA Toolbox (GIFT) (http://mialab.mrn.org) that estimates covarying networks. SBM can be considered as a multivariate extension of VBM which accounts for spatial dependencies among different regions and increases sensitivity to effects distributed across the neuraxis. SBM applies spatial independent component analysis[26] (organised as subjects-by-voxels) to produce maximally independent components (components-by-voxels) and their associated mixing-matrices (subjects-by-components). The number of components (k) for subsequent ICA were estimated using a principled information theoretic approach (rather than arbitrarily selecting the number of components[26]). ICA was then applied to the T1w WM images of 23 HC, 12 NP and 17 without NP, which were arranged into one 53-row (subject-by-T1w-WMvoxels) data matrix. This data matrix was then decomposed into a mixing matrix (subjects by components) and a component matrix (components by voxels). The mixing matrix expresses the relationship between 53 subjects and k components. The rows of the mixing matrix indicate the contribution of each k component to a given subject, whereas the columns indicate how each component contributes to the 53 subjects. The component matrix on the other hand expresses the relationship between the k components and brain/cord voxels. The rows of the component matrix indicate how one component contributes to different voxels, whereas the columns of the component matrix indicate how one voxel contributes to each of the components.

The mixing matrix was used for subsequent statistical analysis, where every column of the mixing matrix quantifies the contribution of each component to the 53 subjects. An ANOVA was applied to each column to assess which components showed a significant group difference, adjusted for covariates of no interest (ie, age, gender, total intracranial volume (TIV) and scanner). A false discovery rate[27] controlling procedure with $q^*=0.05$ was used to assess which components were statistically significant. The significant component that survived FDR correction was thresholded at a value of $|Z|>3$ as described in Xu *et al*[28] and was scaled to unit SD (SBM Z map). A significant component comprises clusters of voxels—with positive and negative values—reflecting group effects in different regions of brain and spinal cord that are interrelated to each other.

SBM was repeated for each of the volumetric and microstructural parameter maps. The number of components estimated were 8, 8, 7, 7, 6, 3, 5, 5 for GM and WM maps from the MRPAGE, R1, R2* and MT maps, respectively. Components with loading scores that differed significantly between either controls and patients or NP patients versus pain-free patients were identified. No significant components were found for MT maps. The significant components were rendered on the MNI-normalised BSC template for appropriate contrasts (controls>patients, patients>controls, NP patients>pain free, pain-free>NP patients) (figures 1 and 2). For illustrative purposes, the GM and WM are represented in the same colour for each modality (eg, volume, R1, R2*) of the significant components.

Finally, in order to explore the association between brain and spinal cord changes and pain intensity in patients with NP, we used SPM's multiple linear regression models adjusting for potentially confounding effects of age, gender, time since injury, TIV and scanner upgrade. The explanatory variables in these analyses were pain intensities (range from 0 to 10), while the response variables were the volumetric and microstructural parameter maps above.

RESULTS

Patients' characteristics and clinical outcomes

The demographics of the patients is shown in table 1. Out of 30 chronic traumatic SCI patients (3.6±6.8 years after the injury), 13 reported NP (mean age: 42.9 years, SD=18.2, range=21–73) and 17 were pain-free (mean age: 46.1 years; SD=14.8, range=19–72). All patients underwent state of the art neurorehabilitation in a specialised SCI centre immediately after their injury. The healthy controls had a mean age of 36.9 years (SD=11.8, range=24.0–66.0). All three groups were comparable with respect to age (ANOVA, p=0.1516) and patient groups did not differ with regard to lesion level (p=0.28) or AIS grade (p=0.18). The mean below level NP intensity was 6.1 (SD=1.9).

Pain-associated changes in SCI patients with NP compared with pain-free SCI patients

In NP patients, atrophic changes associated with NP were observed in the cerebellum, middle temporal gyrus and occipital gyrus, while volume increases were observed in the posterior insula, superior temporal, occipital and middle frontal gyrus when compared with pain-free patients (figure 1A and online supplemental S2). Analysis of the R1 component showed signal decreases in primary motor cortex and DLPFC in NP patients when compared with pain-free patients (figure 2A and online supplemental S3). In NP patients, the R2* component showed increased signal in the cervical cord, thalamus, ACC, PAG and para-hippocampal gyrus, while signal was decreased in the lentiform nucleus and substantia nigra when compared with pain-free patients (figure 2A and online supplemental S4). Note, that trauma-related differences were predominantly visible in the medial thalamus whereas pain-related changes were located in the lateral thalamus.

Magnitude of structural changes is associated with pain intensity

In NP patients, pain intensity was negatively associated with R1 in the PAG (Z-score=4.59, cluster extent voxels=72, p=0.004, FWE corrected) and positively correlated with R2* in the cervical cord (Z-score=4.04, cluster extent voxels=123, p=0.025, FWE corrected) (figure 3).

Trauma-associated changes in SCI patients compared with healthy controls

We first confirmed previous reports showing trauma-induced macrostructural and microstructural changes across the motor,

J Neurol Neurosurg Psychiatry: first published as 10.1136/jnnp-2020-325580 on 26 May 2021. Downloaded from http://jnnp.bmj.com/ on July 20, 2021 at E-Library Insel. Protected by copyright.

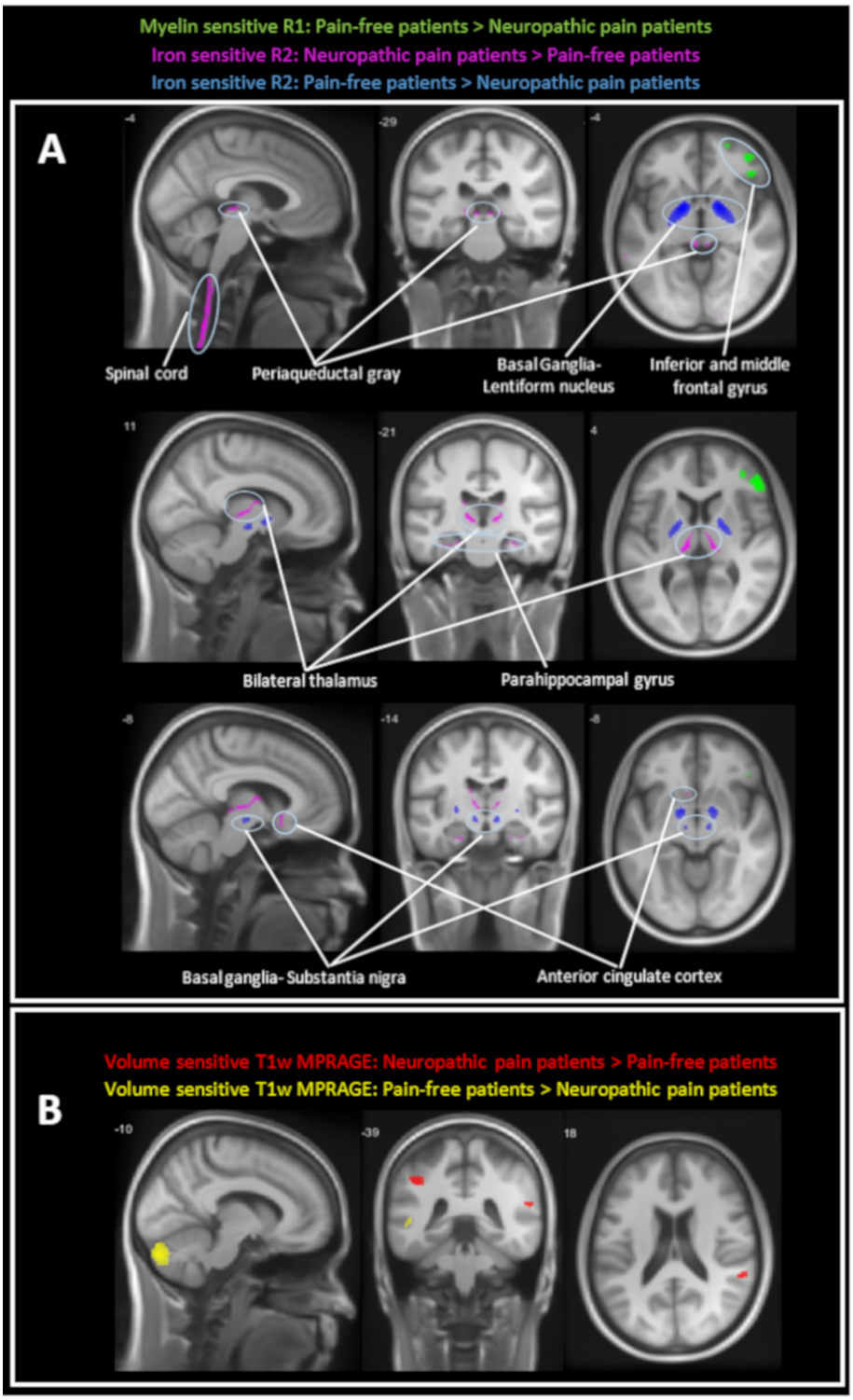

Figure 1 Source-based morphometry renderings showing pain-induced macrostructural and microstructural changes along the neuroaxis, with key areas of the sensorimotor and limbic system affected by atrophy. (A) For patients with neuropathic pain (NP), macrostrucutral (ie, atrophic) changes (shown in yellow) associated with NP were observed in the cerebellum, middle temporal gyrus and occipital gyrus, while volume increases (shown in red) were observed in the posterior insula, superior temporal, occipital and middle frontal gyrus when compared with pain-free patients. (B) For patients with NP when compared with pain-free patients, microstructural changes in terms of longitudinal relaxation (R1) signal decreases were evident in primary motor cortex, dorsolateral prefrontal lobe (shown in green), increase in iron-sensitive effective transverse relaxation rate (R2*) component in the cervical cord, thalamus, anterior cingulate cortex, periaqueductal grey and para-hippocampal gyrus (shown in pink), decrease in R2* (shown in blue) in the basal ganglia (ie, lentiform nucleus) and substantia nigra. MPRAGE, magnetisation-prepared rapid acquisition gradient echo; T1w, T1 weighted.

sensory and limbic system. Specifically, macroscopic changes (decreased volume) were observed in the cervical cord, cerebellum, thalamus, posterior cingulate, lingual gyrus, precuneus, superior and medial temporal gyrus and para-hippocampal gyrus (figures 1B and 2) when all patients (NP+pain free) were compared with controls. In these atrophied areas and beyond,

J Neurol Neurosurg Psychiatry: first published as 10.1136/jnnp-2020-325580 on 26 May 2021. Downloaded from http://jnnp.bmj.com/ on July 20, 2021 at E-Library Insel. Protected by copyright.

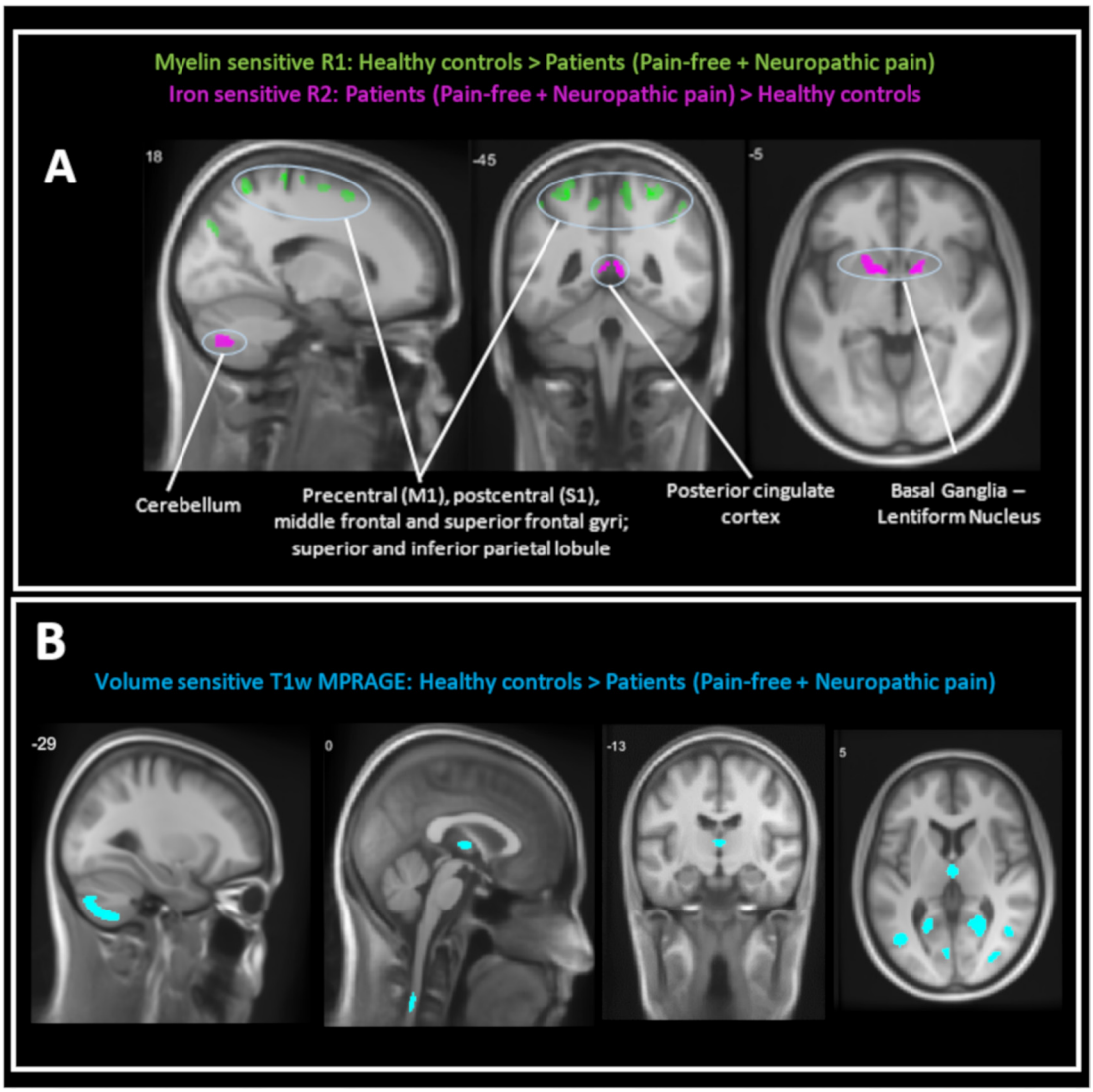

Figure 2 Source-based morphometry renderings showing trauma induced macrostructural and microstructural changes across the motor, sensory and limbic system (|Z|=3) in the brain and spinal cord. (A) Trauma induced volumetric changes (ie, all patients (neuropathic pain (NP)+pain-free) were compared with controls) the cervical cord, thalamus, posterior cingulate, lingual gyrus, precuneus, superior and middle temporal gyrus and para-hippocampal gyrus showed significant atrophy (shown in blue). (B) For patients with and without NP when compared with healthy controls, myelin-sensitive longitudinal relaxation (R1) component (shown in green) was decreased in the sensorimotor cortices, middle frontal gyrus, precuneus and inferior parietal lobule, whereas iron-sensitive effective transverse relaxation rate (R2*) component (shown in pink) showed increases in the cervical cord, lentiform nucleus, cerebellum, posterior cingulate, middle temporal gyrus, right cerebellum and fusiform gyrus. MPRAGE, magnetisation-prepared rapid acquisition gradient echo; T1w, T1 weighted.

R1 component was decreased in the sensorimotor cortices, middle frontal gyrus, precuneus and inferior parietal lobule when compared with healthy controls. The R2* component showed an increase in the cervical cord, lentiform nucleus, cerebellum, posterior cingulate, middle temporal gyrus, right cerebellum and fusiform gyrus (figure 2B and online supplemental S3 and S4).

DISCUSSION

This study shows both decreased and increased myelin-sensitive and iron-sensitive content differences associated specifically with NP along the trajectory of ascending and descending nociceptive pathways after SCI. Most group effects are located within key structures involved in endogenous pain modulation.[4] As SCI provides an ideal model to differentially study trauma-related and pain-related effects—following a defined lesion to the nervous system—these findings speak to specific pathophysiological mechanisms related to the development and maintenance of chronic NP after SCI.

We first dissociated trauma-induced changes from NP associated (micro-)structural changes. In agreement with previous reports, trauma-induced atrophic changes, as well as myelin and iron changes, were evident across the sensorimotor and limbic system (for review, see Freund *et al*[7]). Accompanying trauma-induced changes, volumetric increases and decreases in the cervical cord, thalamus, primary somatosensory cortex, ACC and DLPFC have been also associated with NP following SCI.[9] The neuronal substrates underlying injury-induced volumetric alterations remain incompletely understood. Pathophysiologically, chronic ectopic electrical activity in residual spinothalamic tract axons,[29] upregulation of sodium channels in nociceptive neurons,[30] and increases in pro-inflammatory cytokines[31] are potentialmechanism involved. As volumetric changes

J Neurol Neurosurg Psychiatry: first published as 10.1136/jnnp-2020-325580 on 26 May 2021. Downloaded from http://jnnp.bmj.com/ on July 20, 2021 at E-Library Insel. Protected by copyright.

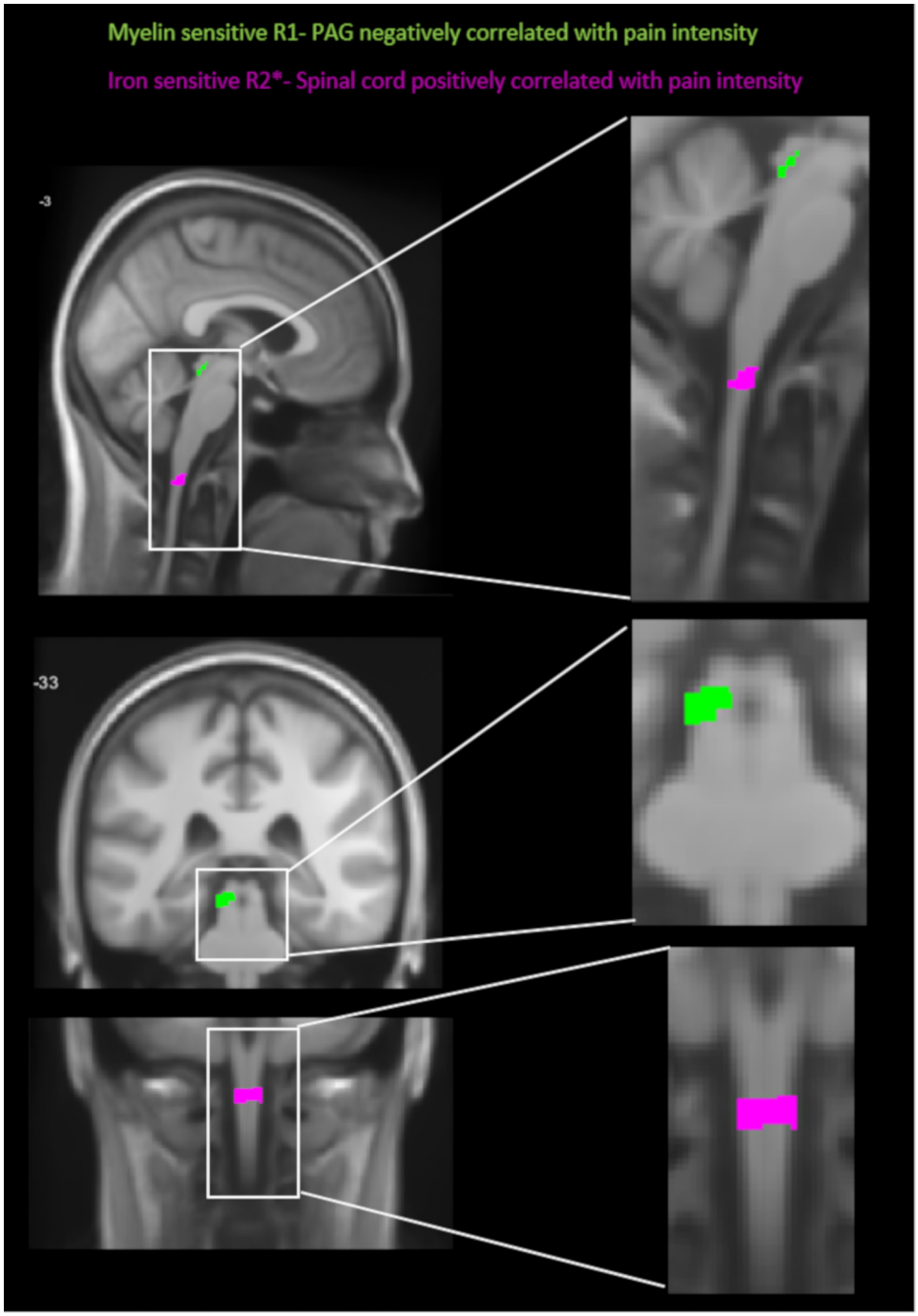

Figure 3 Statistical parametric maps testing (ie, linear regression) for an association between longitudinal relaxation (R1) and effective transverse relaxation rate (R2*) signal changes and pain intensity in the periaqueduct and medulla oblongata (t values uncorrected p<0.005, shown for descriptive purposes, masked by the union of the regions of interest). PAG, periaqueductal grey.

can represent a myriad of physiologically and pathophysiological changes, we sought to reveal the underlying microstructural substrates of such pain-associated volumetric changes by revealing changes in myelin and iron content along the trajectories of ascending and descending nociceptive pathways. Specifically, R2* increases were detectable in the spinal cord, PAG, thalamus, ACC and para-hippocampal gyrus, suggesting iron accumulation due to neurodegenerative processes[13] in regions that have previously been implicated in NP after SCI.[9 18 32] It remains speculative which pathophysiological processes drive changes in R2* contrasts as a range of physiological and pathophysiological processes can contribute to the gradient echo signal decay (and thus R2*). Remyelination, during recovery and reorganisation processes may impact myelin architecture and thereby R2*.[13] Inflammatory processes leading to microglial activation and neurodegenerative processes may result in changes in R2*, but also to changes in metabolic demand affecting the concentration of deoxyhaemoglobin in certain brain areas also influences R2*.[33] However, although there is a complex interplay between myelin, iron accumulation and R2* values in brain pathology, remote spinal cord and brain changes following SCI are likely related to anterograde and retrograde degeneration and subsequent changes in diaschitic regions.

J Neurol Neurosurg Psychiatry: first published as 10.1136/jnnp-2020-325580 on 26 May 2021. Downloaded from http://jnnp.bmj.com/ on July 20, 2021 at E-Library Insel. Protected by copyright.

Communication between the prefrontal cortical areas and the PAG has been recently shown in functional MRI studies.[34] Here, we provide evidence for further downstream effects. Notably, microstructural alterations were detected within the spinal cord and also the PAG. These effects were related to pain intensity; furnishing an important predictive validity to this imaging phenotype. The PAG is known to serve as a link between the forebrain and the lower brainstem and is pivotal for the descending modulation of pain. It receives input from the frontal lobe, amygdala, hypothalamus and ACC and engages the rostral ventral medulla which in turn controls nociceptive processing in the spinal dorsal horn.[35] Direct stimulation of the PAG has successfully been trialled as a treatment option for NP including pain following SCI.[36] Thus, it is anticipated that molecular changes in the PAG could compromise descending inhibition of nociceptive processing and subsequently increase the spinal gain of incoming information. Our study is the first to provide evidence for NP-related changes in PAG microstructure in humans, underscoring the clinical relevance of these changes for NP following SCI. In conjunction with microstructural alteration in the injured spinal cord, these findings are compatible with the notion of a dysfunctional spinal–bulbo–spinal loop, a key circuit of the descending pain modulatory system.[3]

Additional evidence for an impaired descending pain modulatory system can be inferred from microstructural changes in other key constituents of this network, namely the ACC (ie, increased iron accumulation) and DLPFC circuitry[4] (ie, reduced myelin content). Previous studies had found structural and functional NP associations in the DLPFC[37] in those with NP. For example, reduced GM volume and hypometabolisms in the left DLPFC were observed in SCI patients suffering from NP when compared with healthy controls.[38] Here, we not only show that this reduction in volume is linked to a decrease in myelin-sensitive R1, but also that it is pain specific—as this reduction was not observed in pain-free patients. As the DLPFC is both involved in top-down inhibition and facilitation of pain, the decreases in myelin content reported herein align well with the concept of pathological nociceptive gain control in NP after SCI.[2]

The thalamus is considered to play an important role in the pathophysiology of central NP after SCI.[32] After a spinal lesion ascending somatosensory pathways are damaged, which may result in deafferentation of rostral relay structures such as the thalamus. Intriguingly, our finding of R2* signal changes which may reflect iron accumulation in the thalamus in SCI patients with NP was confined to lateral thalamic nuclei, while volumetric changes in the medial thalamus were trauma-related (ie, found in SCI with and without NP). These findings offer an essential line of evidence that structural plasticity within the thalamus is specifically linked to the pathophysiology of NP after SCI.

Finally, we observed an unexpected decrease of iron-sensitive R2* in the basal ganglia. The role of the basal ganglia in chronic pain conditions is still poorly understood, but its vast anatomical connections to a multitude of brain areas (including the thalamus) and cervical cord make it plausible that the basal ganglia could play an important role in aberrant nociceptive bottom-up and top-down signalling (for review, see Borsook *et al*[39]). Our findings warrant further studies into the role of basal ganglia pathways in central NP. At present, the implications of these findings remain highly speculative.

From a technical perspective, the multivariate (SBM) tests for group effects described above are, in principle, much more sensitive than the equivalent mass univariate (VBM) tests one would obtain from analysing the volumetric and microstructural images directly. This is because multivariate analyses do not try to assign a significance to each voxel or region—they test for distributed effects that covary among individuals.[16] Crucially, this multivariate analysis would not have been possible without combining the brain and spinal cord within the same analysis. This speaks to the potential importance of the combined brain and spine template used to spatially normalise our data. This template is available through open access (http://www.fil.ion.ucl.ac.uk/spm/toolbox/TPM/) for related studies that test for distributed effects throughout the neural axis.

LIMITATIONS

Our study had some limitations. The cross-sectional nature of the study restricts conclusions to a single time point and thus the temporal evolution of the above-described microstructural changes remains uncertain. Despite the histological evidence that MT, R1 and R2* markers correspond to their biochemical counterparts[13], they are indirect contrasts of myelin and iron content and any interpretation should take this into consideration.

It should be noted that concurrently observed changes in R2*, R1 and MT may not be apparent in all microstructural changes. First, the sensitivity or signal-to-noise ratio in these different quantitative measures varies significantly.[40] Thus, differences in sensitivity may render these measures complementary, that is, certain changes may only be visible in one of the metrics. Second, the different metrics have a distinct specificity and sensitivity to underlying microstructural changes.[22] For example, R2* is exquisitely sensitive to changes in local susceptibility and concentration of paramagnetic compounds such as iron. Callaghan and colleagues[41] have demonstrated that R1 can be estimated from R2* and MT measurements by a general linear relaxometry model, which demonstrates that R2* and MT changes may even cancel each other and result in zero change in R1. Thus, partial contributions of unexplored physiological/cellular processes occurring after SCI cannot be excluded. Moreover, current standardised neurological tests cannot account for unobserved latent lifestyle or genetic factors which might be different between SCI patients and controls, a-priori. To mitigate any potential effect of the scanner upgrade on our results, we ensured that the same number of patients and controls were measured before and after upgrade, allowing us to account for the upgrade effect (common to both cohorts) and modelled out any linear effect of these covariates of interest. Moreover, Leutritz *et al*[40] demonstrated that the systematic bias in R1, MT and R2* measurements between a Skyra and Verio Siemens scanner setup is <4%. Thus, we are confident that the effects seen in this study are related to pathophysiological changes rather than technical sources. Finally, sex was not balanced across groups, with most of the participants being men. However, this is representative of the general population of SCI patients, in which the male to female patients' ratio is roughly 4:1 and we also adjusted our models for this covariate of no interest.

CONCLUSION

This study evinces the microstructural signature of NP, affecting key constituents of the ascending and descending nociceptive pathways—its magnitude being directly linked to NP intensity. The complex interplay between myelin and iron changes in areas related to sensory and affective processing highlights maladaptive plastic processes likely involved in the maintenance of NP. Beyond unravelling the intimate pathophysiology of NP, tracking microstructural plasticity may facilitate patient monitoring during clinical trials for NP.

Author affiliations
[1]Spinal Cord Injury Center, University Hospital Balgrist, University of Zurich, Zurich, Switzerland

J Neurol Neurosurg Psychiatry: first published as 10.1136/jnnp-2020-325580 on 26 May 2021. Downloaded from http://jnnp.bmj.com/ on July 20, 2021 at E-Library Insel. Protected by copyright.

[2]Department of Neurology, University Hospital Bern, Inselspital, University of Bern, Bern, Switzerland
[3]Tri-institutional Center for Translational Research in Neuroimaging and Data Science (TReNDS): Georgia State University, Georgia Institute of Technology, Emory University, Atlanta, Georgia, USA
[4]Wellcome Centre for Human Neuroimaging, UCL Institute of Neurology, UCL, London, UK
[5]Neurophysics, Max-Planck-Institut fur Kognitions- und Neurowissenschaften, Leipzig, Germany
[6]Wellcome Centre for Integrative Neuroimaging (WIN), Nuffield Department of Clinical Neurosciences, University of Oxford, John Radcliffe Hospital, Oxford, UK
[7]German Center for Neurodegenerative Disease (DZNE), Magdeburg, Germany

Acknowledgements We thank all participants for their time spent and contribution in this study.

Contributors SPK and MA: acquisition, analysis and interpretation of data; writing the manuscript. JR: acquisition, interpretation of data; writing the manuscript. VDC, CB, JA, NW, KW, KF and GZ: interpretation of data, critical revision of manuscript for intellectual content. PF: critical revision of manuscript for intellectual content; study supervision.

Funding NW reports grants from European Research Council/ERC grant agreement n° 616905, grants from BMBF (01EW1711AB) in the framework of ERA-NET NEURON, grants from BRAINTRAIN European research network (Collaborative Project) supported by the European Commission (Grant agreement n° 602186), grants from NISCI supported by the European Union's Horizon 2020 research and innovation programprogramme under the grant agreement No 681094, and supported by the Swiss State Secretariat for Education, Research and Innovation (SERI) under contract number 15.0137, grants from UCL Impact Awards and Siemens Healthcare, during the conduct of the study; and The Wellcome Centre for Human Neuroimaging and Max Planck Institute for Human Cognitive and Brain Sciences have institutional research agreements with Siemens Healthcare. PF reports grants from ERA-NET NEURON (hMRIofSCIno: 32NE30_173678), grants from NISCI supported by the European Union's Horizon 2020 research and innovation programme under the grant agreement No 681094, and supported by the Swiss State Secretariat for Education, Research and Innovation (SERI) under contract number 15.0137, grants from Wings for life charity (No WFL-CH-007/14), grants from International Foundation for Research (IRP-158). PF is funded by an SNF Eccellenza Professorial Fellowship grant (PCEFP3_181362/1). VC reports NIH grants R01EB020407 and R01MH118695. KF is funded by a Wellcome Trust Principal Research Fellowship (Ref: 088130/Z/09/Z). Open access of this publication is supported by the Wellcome Trust (091593/Z/10/Z).

Competing interests The Max Planck Institute for Human Cognitive and Brain Sciences and Wellcome Centre for Human Neuroimaging have institutional research agreements with Siemens Healthcare. NW holds a patent on acquisition of MRI data during spoiler gradients (US 10401453 B2). NW was a speaker at an event organised by Siemens Healthcare and was reimbursed for the travel expenses.

Patient consent for publication Not required.

Ethics approval All participants provided written informed consent prior to enrolment and the study was approved by the Ethics Committee of the Canton Zurich (EK-2010–0271).

Provenance and peer review Not commissioned; externally peer reviewed.

Data availability statement Anonymised grouped data will be shared by request from a qualified investigator.

Supplemental material This content has been supplied by the author(s). It has not been vetted by BMJ Publishing Group Limited (BMJ) and may not have been peer-reviewed. Any opinions or recommendations discussed are solely those of the author(s) and are not endorsed by BMJ. BMJ disclaims all liability and responsibility arising from any reliance placed on the content. Where the content includes any translated material, BMJ does not warrant the accuracy and reliability of the translations (including but not limited to local regulations, clinical guidelines, terminology, drug names and drug dosages), and is not responsible for any error and/or omissions arising from translation and adaptation or otherwise.

Open access This is an open access article distributed in accordance with the Creative Commons Attribution Non Commercial (CC BY-NC 4.0) license, which permits others to distribute, remix, adapt, build upon this work non-commercially, and license their derivative works on different terms, provided the original work is properly cited, appropriate credit is given, any changes made indicated, and the use is non-commercial. See: http://creativecommons.org/licenses/by-nc/4.0/.

ORCID iDs
Jan Rosner http://orcid.org/0000-0002-1973-1773
Patrick Freund http://orcid.org/0000-0002-4851-2246

REFERENCES

1 Colloca L, Ludman T, Bouhassira D, *et al*. Neuropathic pain. *Nat Rev Dis Primers* 2017;3:17002.
2 Albu S, Gómez-Soriano J, Avila-Martin G, *et al*. Deficient conditioned pain modulation after spinal cord injury correlates with clinical spontaneous pain measures. *Pain* 2015;156:260–72.
3 Villanueva L, Le Bars D. The activation of bulbo-spinal controls by peripheral nociceptive inputs: diffuse noxious inhibitory controls. *Biol Res* 1995;28:113–25.
4 Wiech K. Deconstructing the sensation of pain: the influence of cognitive processes on pain perception. *Science* 2016;354:584–7.
5 Bingel U, Tracey I. Imaging CNS modulation of pain in humans. *Physiology* 2008;23:371–80.
6 Treede R-D. Gain control mechanisms in the nociceptive system. *Pain* 2016;157:1199–204.
7 Freund P, Seif M, Weiskopf N, *et al*. MRI in traumatic spinal cord injury: from clinical assessment to neuroimaging biomarkers. *Lancet Neurol* 2019;18:1123–35.
8 Weiskopf N, Suckling J, Williams G, *et al*. Quantitative multi-parameter mapping of R1, PD(*), MT, and R2(*) at 3T: a multi-center validation. *Front Neurosci* 2013;7:95.
9 Jutzeler CR, Huber E, Callaghan MF, *et al*. Association of pain and CNS structural changes after spinal cord injury. *Sci Rep* 2016;6:18534.
10 Pfyffer D, Vallotton K, Curt A, *et al*. Tissue bridges predict neuropathic pain emergence after spinal cord injury. *J Neurol Neurosurg Psychiatry* 2020;91:1111–7.
11 Natu VS, Gomez J, Barnett M, *et al*. Apparent thinning of human visual cortex during childhood is associated with myelination. *Proc Natl Acad Sci U S A* 2019;116:20750–9.
12 Callaghan MF, Freund P, Draganski B, *et al*. Widespread age-related differences in the human brain microstructure revealed by quantitative magnetic resonance imaging. *Neurobiol Aging* 2014;35:1862–72.
13 Langkammer C, Krebs N, Goessler W, *et al*. Quantitative MR imaging of brain iron: a postmortem validation study. *Radiology* 2010;257:455–62.
14 Blaiotta C, Freund P, Cardoso MJ, *et al*. Generative diffeomorphic modelling of large MRI data sets for probabilistic template construction. *Neuroimage* 2018;166:117–34.
15 Kaspárek T, Marecek R, Schwarz D, *et al*. Source-based morphometry of gray matter volume in men with first-episode schizophrenia. *Hum Brain Mapp* 2010;31:300–10.
16 Gupta CN, Turner JA, Calhoun VD. Source-based morphometry: a decade of covarying structural brain patterns. *Brain Struct Funct* 2019;224:3031–44.
17 Freund P, Weiskopf N, Ashburner J, *et al*. MRI investigation of the sensorimotor cortex and the corticospinal tract after acute spinal cord injury: a prospective longitudinal study. *Lancet Neurol* 2013;12:873–81.
18 Ziegler G, Grabher P, Thompson A, *et al*. Progressive neurodegeneration following spinal cord injury. *Neurology* 2018;90:e1257–66.
19 Grabher P, Callaghan MF, Ashburner J, *et al*. Tracking sensory system atrophy and outcome prediction in spinal cord injury. *Ann Neurol* 2015;78:751–61.
20 Kirshblum SC, Waring W, Biering-Sorensen F, *et al*. Reference for the 2011 revision of the International standards for neurological classification of spinal cord injury. *J Spinal Cord Med* 2011;34:547–54.
21 Bryce TN, Biering-Sørensen F, Finnerup NB, *et al*. International spinal cord injury pain classification: Part I. Background and description. March 6-7, 2009. *Spinal Cord* 2012;50:413–7.
22 Weiskopf N, Mohammadi S, Lutti A, *et al*. Advances in MRI-based computational neuroanatomy: from morphometry to in-vivo histology. *Curr Opin Neurol* 2015;28:313–22.
23 Azzarito M, Seif M, Kyathanahally S, *et al*. Tracking the neurodegenerative gradient after spinal cord injury. *Neuroimage Clin* 2020;26:102221.
24 Ashburner J, Friston KJ. Unified segmentation. *Neuroimage* 2005;26:839–51.
25 Ashburner J. A fast diffeomorphic image registration algorithm. *Neuroimage* 2007;38:95–113.
26 Calhoun VD, Adali T, Pearlson GD, *et al*. A method for making group inferences from functional MRI data using independent component analysis. *Hum Brain Mapp* 2001;14:140–51.
27 Benjamini Y, Hochberg Y. Controlling the false discovery rate: a practical and powerful approach to multiple testing. *J R Stat Soc Ser B* 1995;57:289–300.
28 Xu L, Groth KM, Pearlson G, *et al*. Source-based morphometry: the use of independent component analysis to identify gray matter differences with application to schizophrenia. *Hum Brain Mapp* 2009;30:711–24.
29 Djouhri L, Koutsikou S, Fang X, Pain S, Neuropathic B, *et al*. Spontaneous pain, both neuropathic and inflammatory, is related to frequency of spontaneous firing in intact C-fiber nociceptors. *J Neurosci* 2006;26:1281–92.
30 Hains BC, Waxman SG. *Sodium channel expression and the molecular pathophysiology of pain after SCI*. In: Progress in brain research, 2007: 195–203.
31 Detloff MR, Fisher LC, McGaughy V, *et al*. Remote activation of microglia and pro-inflammatory cytokines predict the onset and severity of below-level neuropathic pain after spinal cord injury in rats. *Exp Neurol* 2008;212:337–47.
32 Gustin SM, Wrigley PJ, Youssef AM, *et al*. Thalamic activity and biochemical changes in individuals with neuropathic pain after spinal cord injury. *Pain* 2014;155:1027–36.

J Neurol Neurosurg Psychiatry: first published as 10.1136/jnnp-2020-325580 on 26 May 2021. Downloaded from http://jnnp.bmj.com/ on July 20, 2021 at E-Library Insel. Protected by copyright.

33 Cheng X, Berman AJL, Polimeni JR, *et al*. Dependence of the MR signal on the magnetic susceptibility of blood studied with models based on real microvascular networks. *Magn Reson Med* 2019;81:3865–74.
34 Tinnermann A, Geuter S, Sprenger C, *et al*. Interactions between brain and spinal cord mediate value effects in nocebo hyperalgesia. *Science* 2017;358:105–8.
35 Basbaum AI, Fields HL. The origin of descending pathways in the dorsolateral funiculus of the spinal cord of the cat and rat: further studies on the anatomy of pain modulation. *J Comp Neurol* 1979;187:513–31.
36 Jermakowicz WJ, Hentall ID, Jagid JR, *et al*. Deep brain stimulation improves the symptoms and sensory signs of persistent central neuropathic pain from spinal cord injury: a case report. *Front Hum Neurosci* 2017;11:177.
37 Gustin SM, Wrigley PJ, Siddall PJ, *et al*. Brain anatomy changes associated with persistent neuropathic pain following spinal cord injury. *Cereb Cortex* 2010;20:1409–19.
38 Yoon EJ, Kim YK, Shin HI, *et al*. Cortical and white matter alterations in patients with neuropathic pain after spinal cord injury. *Brain Res* 2013;1540:64–73.
39 Borsook D, Upadhyay J, Chudler EH, *et al*. A key role of the basal ganglia in pain and analgesia--insights gained through human functional imaging. *Mol Pain* 2010;6:27.
40 Leutritz T, Seif M, Helms G. Multiparameter mapping of relaxation (R1, R2*), proton density and magnetization transfer saturation at 3 T: a multicenter dual-vendor reproducibility and repeatability study. *Hum Brain Mapp* 2020.
41 Callaghan MF, Helms G, Lutti A, *et al*. A general linear relaxometry model of R1 using imaging data. *Magn Reson Med* 2015;73:1309–14.

J Neurol Neurosurg Psychiatry: first published as 10.1136/jnnp-2020-325580 on 26 May 2021. Downloaded from http://jnnp.bmj.com/ on July 20, 2021 at E-Library Insel. Protected by copyright.